Design and Construction of a Surface Encoder with Dual Sine-Grids

Akihide Kimura[1,#], Wei Gao[1] and Satoshi Kiyono[1]

1 Department of Nanomechanics, Tohoku University, Sendai 980-8579, Japan
Corresponding Author / E-mail: kimura@nano.mech.tohoku.ac.jp; TEL: +81-22-795-6953; FAX: +81-22-795-6953

KEYWORDS: Surface encoder, Position detection, Measurement, Optical sensor, Nanometer

This paper describes a second-generation dual sine-grid surface encoder for 2-D position measurements. The surface encoder consisted of a 2-D grid with a 2-D sinusoidal pattern on its surface, and a 2-D angle sensor that detected the 2-D profile of the surface grid. The 2-D angle sensor design of previously developed first-generation surface encoders was based on geometric optics. To improve the resolution of the surface encoder, we fabricated a 2-D sine-grid with a pitch of 10 μm. We also established a new optical model for the second-generation surface encoder that utilizes diffraction and interference to generate its measured values. The 2-D sine-grid was fabricated on a workpiece by an ultraprecision lathe with the assistance of a fast tool servo. We then performed a UV-casting process to imprint the sine-grid on a transparent plastic film and constructed an experimental setup to realize the second-generation surface encoder. We conducted tests that demonstrated the feasibility of the proposed surface encoder model.

Manuscript received: May 1, 2006 / Accepted: November 22, 2006

1. Introduction

Precision XY stages are key components in semiconductor manufacturing and inspection systems, precision machining systems, and precision measuring instruments.[1,2] It is necessary measure the position of these stages in the x and y directions to provide feedback control.[3,4]

Typically, two-axis laser interferometers are employed to measure the positions of XY stages. Measurement systems using laser interferometers have high levels of resolution and wide measurement ranges[5] but they are also large, complicated, and expensive[6] The accuracy of a laser interferometer is influenced by environmental factors, such as air pressure variations and temperature changes.[7] It is also necessary to use additional sensors, such as rotary encoders or autocollimeters, to measure the tilt and rotary motions of the stage, which makes the positioning unit more complicated, expensive, and difficult to integrate into precision systems.

A surface encoder, which consists of a two-dimensional (2-D) sine-grid and a 2-D angle sensor, has been proposed as an alternative device to a laser interferometer.[8,9] A surface encoder can measure XY displacements by detecting 2-D sinusoidal patterns on the 2-D sine-grid with its 2-D angle sensor. Tilt and rotation motions can also be detected by scanning multi-spot beams on the 2-D sine-grid or by adding extra 2-D angle sensors.[10,11]

The resolution of a surface encoder is 20 nm in the x and y directions.[12] Recently, the requirement for more precise measurements has led to an urgent demand to improve this resolution. This requires a reduction in the pitch of the 2-D sine-grid. However, the diffraction must also be considered as the pitch is shortened. In this study, we fabricated a 2-D sine-grid with a shortened pitch, and designed and constructed a new optical sensor based on wave-optics to improve the resolution of surface encoders.

2. Surface encoders

This section introduces the principles of conventional first-generation surface encoders and describes two approaches for improving their resolution.

2.1 Principle of a first-generation surface encoder

Figure 1 shows a schematic view of a first-generation surface encoder. It is composed of a 2-D sine-grid with 2-D sinusoidal waves on its surface, and a 2-D angle sensor. A laser beam from a laser diode travels to the 2-D sine-gird through a polarization beam splitter (PBS) and a quadrant wave plate (1/4-λ plate), and is reflected in a certain direction by the local slope of the grid. The laser beam is then collected on a focal plane of a lens after it reflected again by the PBS and the 1/4-λ plate.

The 2-D sine-grid provides a position scale for the surface encoder. Its surface profile can be expressed as

$$h(x,y) = A\,sin\left(\frac{2\pi x}{P}\right) + A\,sin\left(\frac{2\pi y}{P}\right), \tag{1}$$

where P is the pitch of the periodic sine waves in both the x and y directions and A is their amplitude.

The 2-D angle sensor can detect the local slope profiles of the grid surface. It employs the autocollimation technique,[13,14] in which the relationship between the local slope of surface θ and a spot position on the focal plane of the lens d is

Copyright (c) 2007 by KSPE

$$\frac{d}{f} = 2 \cdot \theta, \tag{2}$$

where f is the focal length of the lens. In first-generation surface encoders, the local slopes of the sine grid profile $f(x)$ and $g(y)$ are detected and expressed as the differential of the grid profile $h(x,y)$, so that the following equations can be obtained:

$$\frac{dx}{f} = 2 \cdot f(x) = 2 \cdot \frac{\partial h(x,y)}{\partial x} = 2 \cdot 2\pi A \cos\left(\frac{2\pi x}{P}\right), \text{ and} \tag{3}$$

$$\frac{dy}{f} = 2 \cdot g(y) = 2 \cdot \frac{\partial h(x,y)}{\partial y} = 2 \cdot 2\pi A \cos\left(\frac{2\pi y}{P}\right). \tag{4}$$

Here, (dx,dy) is a spot position on the focal plane. If the spot position is known, the present position (x,y) can be calculated from Equations (3) and (4). Usually, a quadrant photodiode (QPD) or a position sensitive detector (PSD) is preset on the focal plane to detect the spot position.

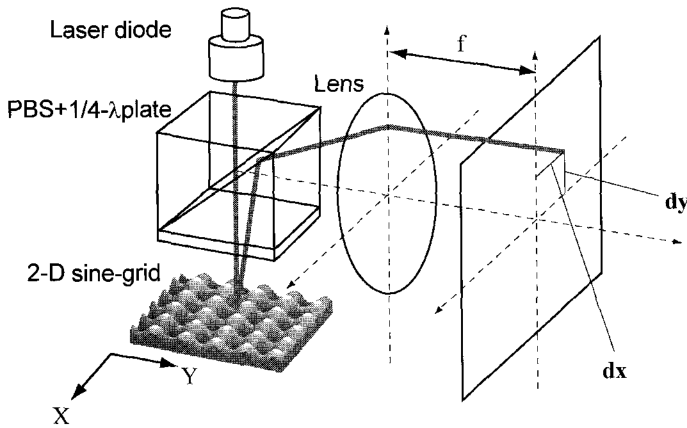

Fig. 1 Schematic of the first generation surface encoder

2.2 Approaches for improving the resolution

To improve the resolution of a surface encoder, it is necessary to shorten the pitch of the 2-D sine-grid. Present surface encoders have a pitch, P, of at least 100 μm [15] The aim of this study was to achieve a P of 10 μm, or 1/10 of the former scale. However, if the pitch of the grid is shortened, the influence caused by diffraction becomes evident and the autocollimation method does not work.

As a result, two important efforts were performed to improve the resolution of the surface encoder. First, a 2-D sine-grid with a short pitch was fabricated. Then a new optical system based on wave optics was developed.

3. Principle of the new encoder

3.1 Fabrication principle of a short-pitch 2-D sine-grid

The 2-D sine-grid was fabricated on a cylindrical workpiece using the system shown in Fig. 2. A fast tool servo (FTS) is a unit that can control the cutting depth of a diamond tool with a piezoelectric driver (PZT) .[15-17] The cutting depth at each point is calculated and stored in a PC before fabrication. In the coordinate configuration shown in Fig. 3, the position of the diamond tool can be expressed as

$$\theta(i) = \frac{2\pi}{N} i, \qquad x(i) = \frac{V_X}{NT} i \tag{5}$$

where N is the pulse number of the rotary encoder of the spindle, i is the ith rotary encoder pulse, T is the rotational speed of the spindle per minute, and V_x is the feed rate of the X-slide in mm/min. To fabricate the 2-D sine-grid defined by Equation (1) on the cylindrical workpiece, the cutting depth $f(i)$ at each point is

$$f(i) = f(\theta(i), x(i)) = A \sin\left(\frac{2\pi r}{P} \frac{2\pi}{N} i\right) + A \sin\left(\frac{2\pi}{P} \frac{Vx}{NT} i\right), \tag{6}$$

where r is the radius of the workpiece.

At the start of fabrication, the data were input in the PZT tube in the form of a voltage, synchronized with the rotary encoder signal of the spindle. A capacitance probe was placed inside the PZT tube to monitor the displacement of the PZT. An analog PID controller provided the feedback control for the PZT.

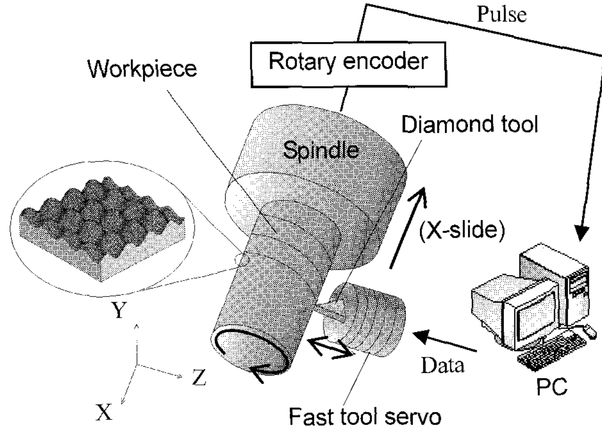

Fig. 2 Schematic diagram of the fabrication system

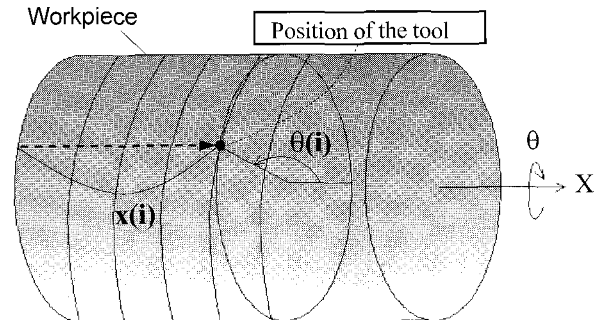

Fig. 3 Coordinate configuration of the workpiece

When the pitch of the grid was shortened, a profile error occurred due to the interference between the diamond tool and the workpiece. Therefore, the shape variation of the diamond tool must be considered to fabricate the desired profile.

The geometric conditions of a diamond tool are shown in Fig. 4. The corner curve R must be smaller than the largest radius of curvature of the sine curve R_{max} (Fig. 4(a)). R_{max} is obtained from

$$R_{max} = \frac{1}{ak^2}, \tag{7}$$

where k is the wave number defined as

$$k = \frac{2\pi}{P}. \tag{8}$$

Thus, the geometric condition of the corner curve must be

$$R < R_{max} = \frac{1}{ak^2}. \tag{9}$$

The clearance angle θ must be larger than $arctan(4A/P)$ (Fig. 4(b)). Then the geometric condition of the clearance angle is

$$\theta > tan^{-1}\left(\frac{4A}{P}\right). \quad (10)$$

The geometric conditions of the diamond tool must satisfy both Equations (9) and (10).

A UV casting technique was performed to replicate the profile of the grid surface on a plane, as shown in Fig. 5. The UV casting provided a high degree of accuracy and could be achieved at room temperature and low pressures.[18,19] A UV resin was poured in the liquid state between the workpiece and the PET film, and UV light was applied above the workpiece. The profile of the grid surface was molded on the PET film, producing a transparent 2-D sine-grid.

3.2 Development of the new optical system

Figure 6 shows a schematic illustration of the developed optical system for the second-generation surface encoder. A second 2-D sine-grid is used in addition to the position scale grid. A laser beam is focused on the first grid and diffracted. As the diffracted beams reach the second grid, they are individually diffracted, as shown in Fig. 6. The diffracted beams finally reach a lens, where beams in the same direction are collected and interfere at the same spot on the focal plane. If the laser is only diffracted in the two directions 0, and +1, the light wave $exp(i\Phi_1)$ (0 and +1 diffracted beam) and the light wave $exp(i\Omega_1)$ (+1 and 0 diffracted beam) interfere at spot I1. The resulting amplitude $U1$ of the sum of both light waves is

$$U1 = exp(i\Phi_1) + exp(i\Omega_1), \quad (11)$$

where Ω_n is a phase difference caused by the optical path difference between the n order beam and 0 order beam,

$$\Omega_n = \frac{2\pi}{\lambda} z\left\{\left(cos\frac{n\lambda}{P}\right)^{-1} - 1\right\}, \quad (12)$$

z is the distance between the two grids, λ is the wavelength of the laser, and Φ_n is a phase shift of the order of diffraction n for the relative displacement x between the grid and diffracted beam. A relationship exists among these parameters:

$$\Phi_n = n \cdot \frac{2\pi x}{P}. \quad (13)$$

The intensity of spot I1 is given by

$$I1 = U1 \cdot \overline{U1} = 2\{1 + cos(\Phi_1 - \Omega_1)\}, \quad (14)$$

where I_1 is a function of the displacement x. While first-generation surface encoders produce their measured value by detecting the local slope of the position scale grid, second-generation surface encoders generate their measured value from the interference of diffracted beams. The best way to achieve this is by using a reflective surface for the position scale grid. However, in this study, the basic experiment was performed with a transparent position scale grid because of the UV casting technique used to generate the 2-D sine grid described in Section 3.1.

3.3 Simulation

In Section 3.2, we only considered diffracted beams in the two directions 0, and +1. However, the beam is diffracted in various orders. As a result, some light waves will interfere at the same spot. For example, at the +1 spot, the −1 and +2 diffracted beam or the +2 and −1 diffracted beam can interfere, in addition to $exp(i\Phi_1)$ and $exp(i\Omega_1)$ given in Equation (11). The interference of the light waves causes a distorted signal.

The diffraction efficiency depends on the amplitude A of the grid, and it is necessary to determine A to obtain a proper sine-wave signal. An optical model of the second-generation surface encoder was constructed as shown in Fig. 7 and used to calculate the intensity of spot I1.

The transparent 2-D sine-grid can be treated as a phase grating that has a phase shifting function. The intensity of the n order diffraction beam is given by

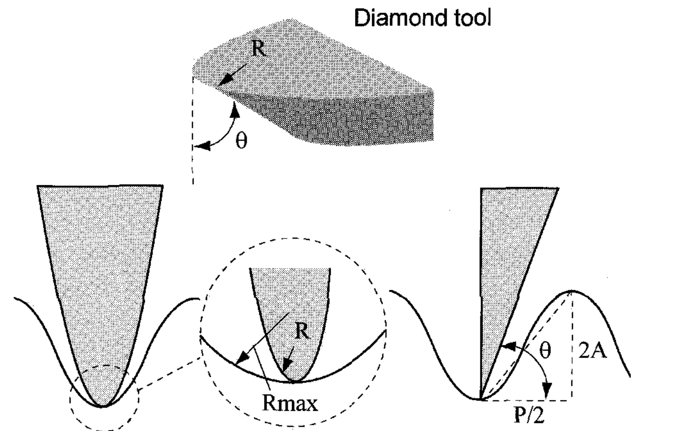

Fig. 4(a) Corner curve Fig. 4(b) Clearance angle

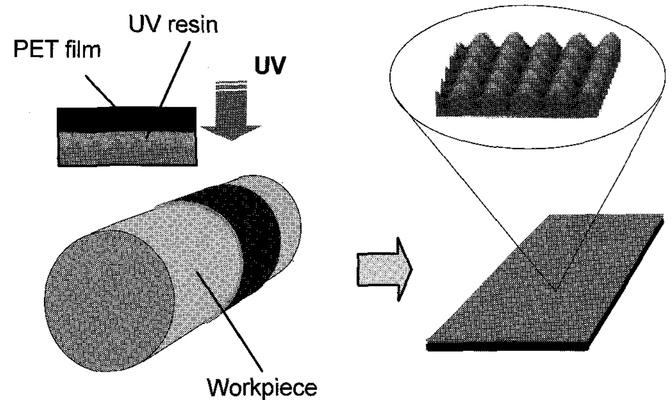

Fig. 5 Schematic diagram of the UV casting

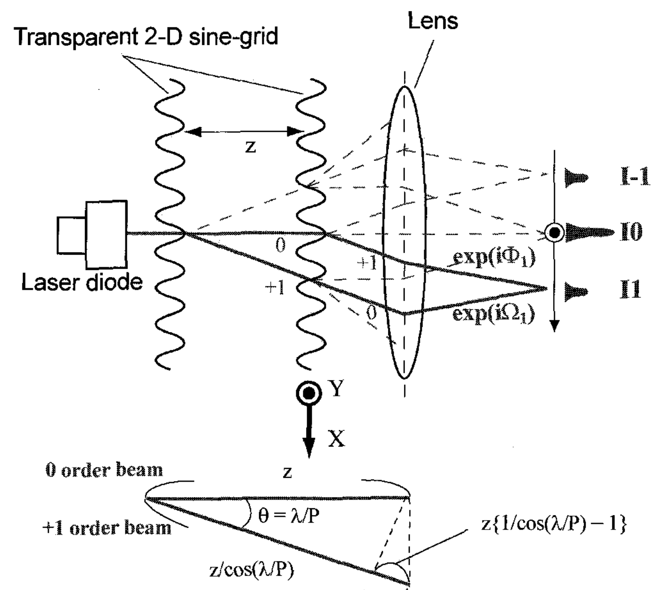

Fig. 6 Second-generation surface encoder

$$u_n = exp\left(\frac{in\pi}{2}\right) \cdot J_n\{(r-1)A\}, \quad (15)$$

where J_n is a Bessel function and r is the reflective index of the UV

resin ($r = 1.5$). The n order diffraction beam $u(1)_n$ of the first grid can be expressed as

$$u(1)_n = exp\left(\frac{in\pi}{2}\right) \cdot J_n\{(r-1)A\} \cdot exp(i\Omega_n) \cdot \tag{16}$$

Equation (16) considers the phase difference caused by the optical path difference between the n order beam and 0 order beam (Equation (12)). The n order diffraction beam $u(2)_n$ of the first grid can be expressed as

$$u(2)_n = exp\left(\frac{in\pi}{2}\right) \cdot J_n\{(r-1)A\} \cdot exp(i\Phi_n) \cdot \tag{17}$$

Equation (17) considers the phase shift of the displacement of the grid (Equation (13)). Beams in the various directions are collected at the same spot on the focal plane of the lens. Thus, the sum of the light waves Un at the +n spot is

$$Un = \sum_m u(1)_m \cdot u(2)_{n-m} \cdot \tag{18}$$

The intensity at spot In is given by

$$In = Un \cdot \overline{Un} \cdot \tag{19}$$

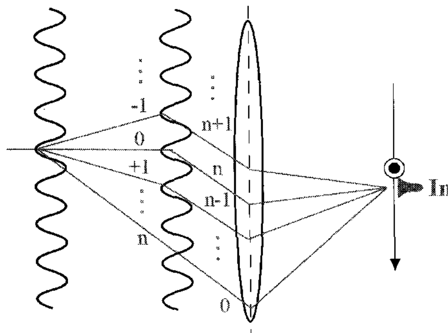

Fig. 7 Optical model of the second-generation surface encoder

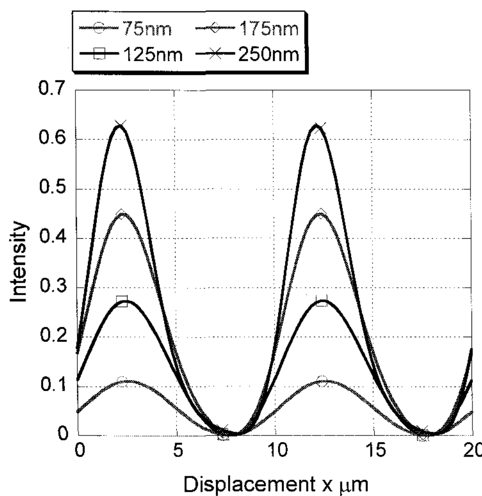

Fig. 8(a) Calculated output of spot I1

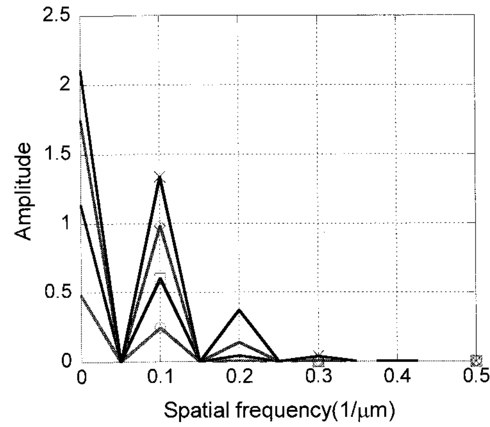

Fig. 8(b) Fourier transformed result of (a)

4. Experiment

4.1 Grid fabrication results

Figure 8 shows the calculated output of I_1 together with its Fourier transformed result. Here, A is 125 nm, which was calculated from the intensity and distortion of the signal.

From Equations (9) and (10), the corner curve R must be smaller than 20 μm and the clearance angle θ must be larger than 3 degrees. Therefore, the diamond tool shown in Fig. 9 was selected. Table 1 shows the specifications of the diamond tool. Its corner curve was 8 μm and its clearance angle was 30 degrees. The fabrication system is shown in Fig. 10 and the fabrication parameters are listed in Table 2. The system was composed of a FTS unit, an ultraprecision lathe (ULC-100A Toshiba Machine Co., Ltd.), and a PC in which the cutting depth data were stored. Figure shows an image of the workpiece after fabrication (VH-9500 Keyence Co., Ltd.).

The UV casting conditions are given in Table 3. The master had the workpiece fabricated on its surface, and the PET film was attached to the workpiece with tape. UV light was applied for 5 minutes until the surface profile was replicated on a 10-mm × 40-mm field. An AFM (Seiko Instruments) image of the replicated film is shown in Fig. 12. The figure shows that a 2-D sine-grid with a pitch of 10 μm and an amplitude of 125 nm was generated on the plane.

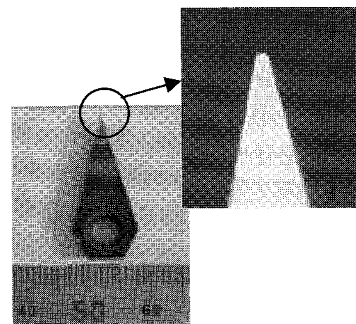

Fig. 9 Photograph of the diamond tool

Table 1 Specifications of the diamond tool

Model	PF-3Z115 Allied Material Co.
Corner curve	8 μm
Clearance angle	30 degrees
Point angle	30 degrees

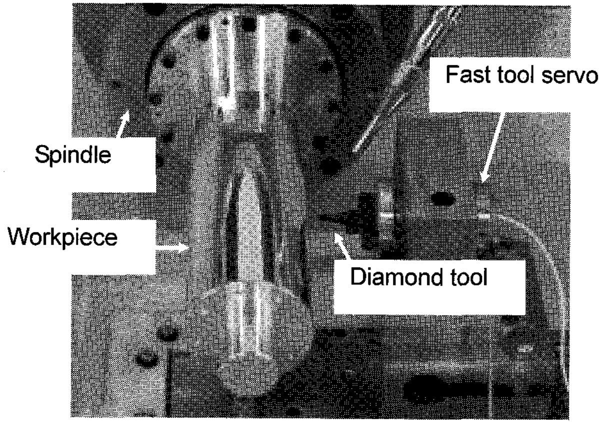

Fig. 10 Photograph of the fabrication system

Table 2 Fabrication conditions

Rotational speed of the spindle	5 rpm
Pulse number of the rotary encoder	180,000 P/rev
Feed rate of the X-slide	1 μm/rev
Diameter of the workpiece	55 mm
Length of the workpiece	150 mm
Material	Aluminum

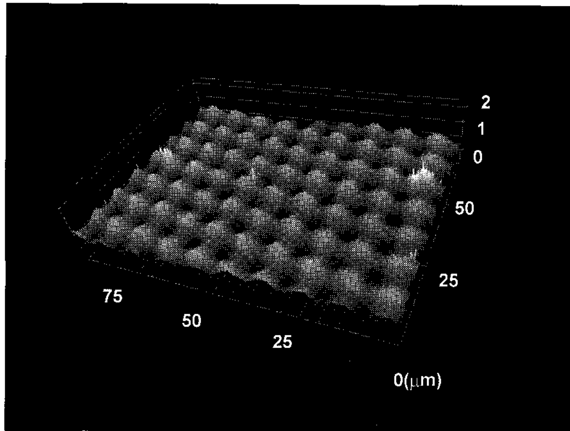

Fig. 11(a) 3-D view of the workpiece image

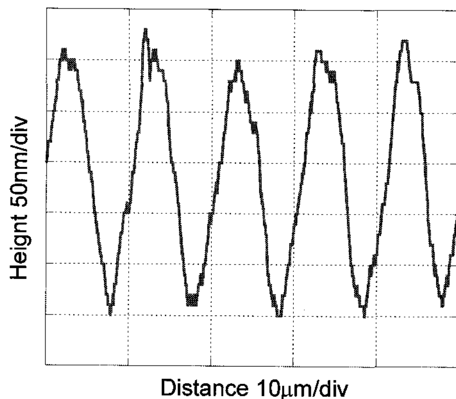

Fig. 11(b) Cross view of the workpiece image

Table 3 Replication conditions

Master	2-D sine-grid on the cylindrical workpiece Pitch: 10 μm Amplitude: 125 nm
Resin	UV resin (Norland Products Inc.)
Film	PET film 140 mm × 40 mm Thickness: 100 μm
Intensity of the UV light	8 mW/ cm^2
Time that the UV light was applied	5 minutes

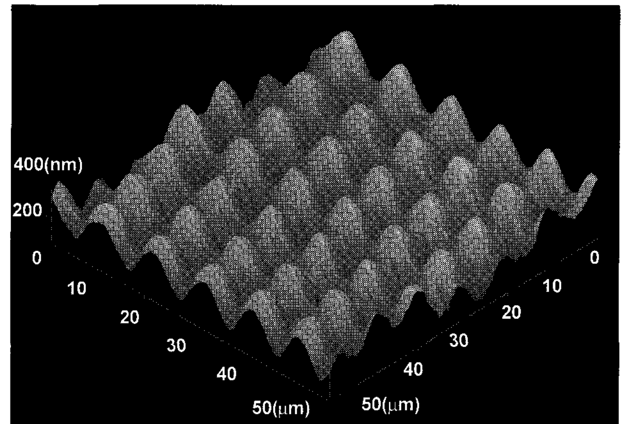

Fig. 12(a) 3-D view of the image of the replicated film

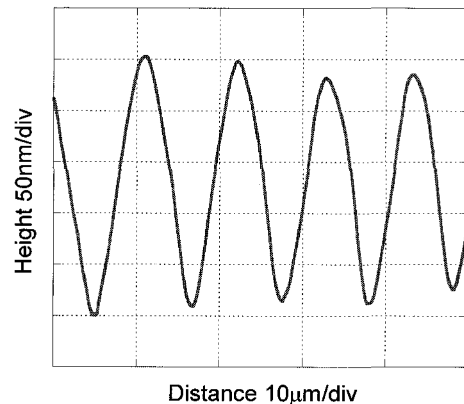

Fig. 12(b) Cross view of the image of the replicated film

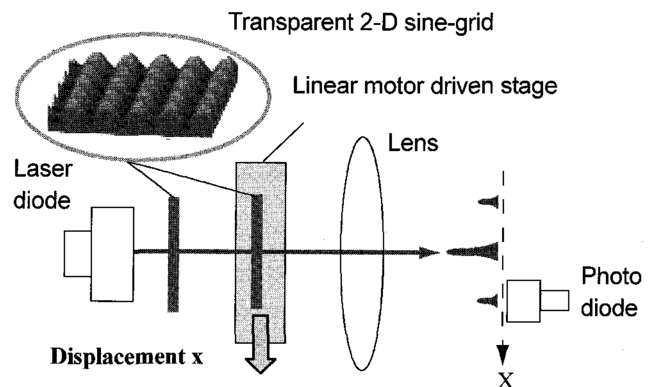

Fig. 13 Schematic diagram of the experimental setup

4.2 Experimental results of the second-generation surface encoder

The experimental setup is schematically shown in Fig. 13. The wavelength of the laser was 685 nm, and the focal distance of the lens was 40 mm. The photoelectric current from the photodiode was converted to a voltage by an I/V converter circuit, passed through an A/D converter, and then stored by the PC. Two transparent 2-D sine-grids were made using the UV casting technique. One grid was placed on the linear motor-driven stage. The displacement of the stage was obtained from a linear encoder (Sony Precision Co., Ltd.). Figure 14 shows the stage movement and the output of spot I1. A signal with a 10-μm period was obtained. The AC/DC ratio in the experimental result was less than that of the simulation due to deviations of the XY axes between the two grids.

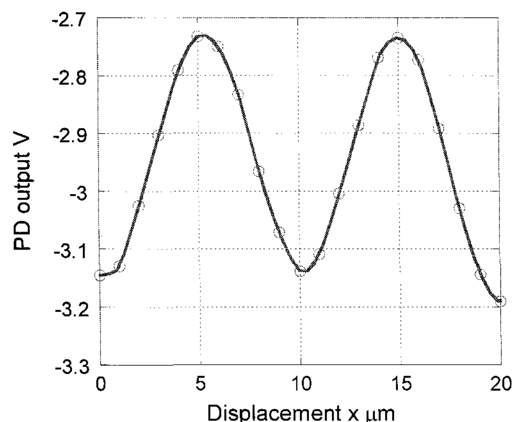

Fig. 14 Experimental results

5. Conclusions

We fabricated a 2-D sine-grid with pitch of 10 μm and developed a new optical system to improve the resolution of surface encoders.

The 2-D sine-grid was fabricated on a cylindrical workpiece with the assistance of a FTS. To fabricate the shortened-pitch 2-D sine-grid, it was necessary to select a diamond tool with a corner curve of 8 μm and a clearance angle of 30 degrees according to the geometric conditions. We performed a UV casting and obtained the profile of the 2-D sine-grid on the PET film.

We designed and constructed a new optical system for the surface encoder. The proposed encoder utilized diffraction and interference to produce its measured value. We performed an experiment and obtained an interference signal with a period of 10 μm. The feasibility of the proposed surface encoder model was demonstrated by the experimental results.

ACKNOWLEDGMENTS

This work was financially supported by a grant from the Japan Society for the Promotion of Science (JSPS). The authors thank B. Ju for his contributions.

REFERENCES

1. Shamoto, E., Murase, H. and Moriwaki, T., "Ultraprecision 6-axis table driven by the means of a walking drive," Annals of the CIRP, Vol. 49, No. 1, pp. 299–302, 2000.

2. Hocken, R. J., Trumper, D. L. and Wang, C., "Dynamics and control of the UNCC/MIT sub-atomic measuring machine," Annals of CIRP, Vol. 50, No. 1, pp. 373–376, 2001.

3. Kim, W. J. and Trumper, D. L., "High precision magnetic levitation stage for photolithography," Precision Engineering, Vol. 22, No. 2, pp. 66–77, 1998.

4. Fan, K. C. and Chen, M. J., "A 6-degree-of-freedom measurement system for the accuracy of X–Y stages," Precision Engineering, Vol. 24, pp. 15–23, 2000.

5. Kao, C. F., Lu, S. H. and Lu, M. H., "High resolution planar encoder by retro-reflection," Review of Scientific Instruments, Vol. 76, No. 085110, pp. 1–7, 2005.

6. Schatten, M. L. and Smith, H. I., "The critical role of metrology in nanotechnology," Proceedings of the SPIE Workshop on Nanostructure Science, Metrology and Technology, Vol. 4608, pp. 1–9, 2001.

7. Teimel, A., "Technology and applications of grating interferometers in high-precision measurement," Precision Engineering, Vol. 14, No. 3, pp. 147–154, 1992.

8. Kiyono, S., Cai, P. and Gao, W., "An angle-based position detection method for precision machines," JSME International Journal, Vol. 42, No. 1, pp. 44–48, 1999.

9. Kiyono, S., Gao, W., Kanai, M., Hoshino, T. and Shimizu, Y., "A new method of position detection using an optical scanning angle sensor," JSME International Journal, Vol. 67, No. 3, pp. 493–497, 2001.

10. Gao, W., Dejima, S., Shimizu, Y. and Kiyono, S., "Precision positioning of two-axis positions and tilt motions using a surface encoder," Annals of CIRP, Vol. 52, No. 1, pp. 435–438, 2003.

11. Dejima, S., Gao, W., Shimizu, H. and Kiyono, S., "Precision positioning of a five degree-of-freedom planar motion stage," Mechatronics, Vol. 15, pp. 969–987, 2005.

12. Gao, W., Dejima, S., Yanai, H., Katakura, K., Kiyono, S. and Tomita, Y., "A surface motor-driven planer motion stage integrated with an XYθz surface encoder for precision positioning," Precision Engineering, Vol. 28, No. 3, pp. 329–337, 2004.

13. Gao, W., Kiyono, S. and Satoh, E., "Precision measurement of multi-degree-of-freedom spindle errors using two-dimensional slope sensors," Annals of CIRP, Vol. 51, No. 1, pp. 447–450, 2002.

14. Gao, W., Huang, P. S., Yamada, T. and Kiyono, S., "A compact and sensitive two-dimensional angle probe for flatness measurement of large silicon wafers," Precision Engineering, Vol. 26, No. 4, pp. 396–404, 2002.

15. Gao, W., Araki, T., Kiyono, S., Okazaki, Y. and Yamanaka, M., "Precision nano-fabrication and evaluation of a large area sinusoidal grid surface for a surface encoder," Precision Engineering, Vol. 27, No. 3, pp. 289–298, 2003.

16. Dow, T. A., Miller, M. H. and Falter, P. J., "Application of a fast tool servo for diamond turning of nonrotationally symmetric surfaces," Precision Engineering, Vol. 13, No. 4, pp. 243–250, 1991.

17. Miller, M. H., Gattard, K. P., Dow, T. A. and Taylor, L. W., "A controller architecture for integrating a fast tool servo into a diamond turning machine," Precision Engineering, Vol. 16, No. 1, pp. 42–48, 1994.

18. Kim, S. and Kang, S., "Replication qualities and optical properties of UV-moulded microlens arrays," Journal of Physics D: Applied Physics, Vol. 36, pp. 2451–2456, 2003.

19. Kang, S., "Replication Technology for Micro/Nano Optical Components," Japanese Journal of Applied Physics, Vol. 43, No. 8B, pp. 5706–5716, 2004.